Present-day velocity and stress fields of the Amurian plate from thin-shell finite element modeling

Carole Petit, Marc Fournier

Geophys. J. Int. (2005) **160,** 357–369 doi: 10.1111/j.1365-246X.2004.02486.x

Present-day velocity and stress fields of the Amurian Plate from thin-shell finite-element modelling

Carole Petit and Marc Fournier

Laboratoire de Tectonique CNRS UMR 7072, *Université Pierre et Marie Curie,* 4 *place Jussieu, Boîte* 129, 75252 *Paris Cedex 05, France.*
E-mail: carole.petit@lgs.jussieu.fr

Accepted 2004 September 20. Received 2004 July 22; in original form 2003 July 25

SUMMARY

Most numerical models of Asian deformation focus on rapidly deforming zones close to the Indian indenter, and seldom extend to its northern 'deformation front'. In this study, we examine the present-day deformation of the Amurian continental plate (northeast Asia) which faces stable Eurasia along the Baikal–Stanovoy boundary. The present-day velocity and stress fields of the Amurian Plate are reproduced by means of thin-shell finite-element modelling. We first compile available GPS and focal mechanism data in and around the Amurian Plate in order to characterize the nature and geometry of its boundaries and its relative velocity with respect to adjacent plates. We then use the finite-element code SHELLS to model the plate deformation under different boundary conditions. Plate rheology, thermal state and crust and mantle thicknesses are fixed according to existing data. We first test the influence of body forces due to crustal thickness variations; then, we test the role of far-field conditions imposed by indentation and extrusion processes to the south, and subduction to the east. Our best-fitting model shows the following. (1) Assuming a relatively 'strong' classical mantle rheology, body forces play a minor role in plate deformation, since they predict velocities much smaller than boundary forces. (2) Transition from south–north compression in the west, to west–east extrusion in the east along the southern plate boundary satisfyingly explains the velocity and stress fields of the Mongolia–Baikal region, suggesting that extrusion is the dominant driving force of the Baikal rift opening. (3) A low-friction fault with null relative Okhotsk–Eurasia and Philippine Sea–Eurasia velocities along the eastern plate limit explain observed stresses and velocities in Sakhalin and Japan, suggesting that eastern subduction processes do not play a major role in long-term plate deformation.

Key words: Amurian Plate, Asian deformation, finite-element models, GPS, stress field.

1 INTRODUCTION

The kinematics of Asia and its interpretation in terms of diffuse or localized deformation have long been a matter of debate, whether one considers finite or instantaneous deformation (e.g. Tapponnier *et al.* 1982; England & Houseman 1986; Avouac & Tapponnier 1993; Houseman & England 1993; Peltzer & Saucier 1996; England & Molnar 1997; Holt *et al.* 2000; Flesch *et al.* 2001). Space geodetic measurements are now widely used to constrain the kinematics of crustal deformation in continental domains, and during the last decade numerous geodetic studies provided key constraints to the deformation of Asia (e.g. Molnar & Gipson 1996; Heki 1996; Crétaux *et al.* 1998; Chamot-Rooke & Le Pichon 1999; Heki *et al.* 1999; Larson *et al.* 1999; Shen *et al.* 2000; Holt *et al.* 2000; Wang *et al.* 2001; Calais *et al.* 2003; Kreemer *et al.* 2003). Among other results, it has been shown that east of longitude 100°E, southeastern and eastern Asia, including Sundaland, South China, North China and the Amurian Plate, move eastward at a mean rate of $\sim$1 cm yr^{-1} relative to Siberia. The relative motions between the main continental blocks of eastern Asia are low, of the order of a few mm yr^{-1}. Thus, a wide region extending from the Baikal Rift to the Japan Sea and to southeast Asia and Indonesia is slowly being extruded eastward at a rate of $\sim$1 cm yr^{-1}. It is now accepted that eastward extrusion of such continental blocks accounts for about a quarter of deformation in Asia, while the remaining three-quarters are accommodated by crustal and/or lithospheric thickening (e.g. Houseman & England 1993; Peltzer & Saucier 1996). As a consequence, any dynamic model of deformation in Asia should take into account body forces due to plate thickening as well as boundary forces coming from the India–Asia collision and Pacific subduction.

Furthermore, the rigid plate assumption may not be valid throughout the continental domain. Recently, the global strain rate model (GSRM) (Kreemer *et al.* 2003) attempted to overcome this problem by defining deformed zones of variable width surrounding *a priori* stable plates. Another dynamic approach is to define a plate rheology and model its deformation and kinematics using boundary velocity conditions given by geodetic and seismological studies. Such numerical models have aimed to reproduce present-day stress

and velocity fields in Asia using continuous or discrete modes of deformation and body and boundary forces (Kong & Bird 1996; Flesch *et al.* 2001). Most of them successfully describe the observed stress and velocity fields in places where deformation is most intense, i.e. the Himalaya and Tibet, Tien Shan, etc. In the remote northern part of the India–Asia collision zone, i.e. in western Mongolia and the Baikal Rift zone, these models are less accurate and predict velocities which are either too low ($\sim$1 mm yr^{-1}, Flesch *et al.* 2001) or too high (19 mm yr^{-1}, Kong & Bird 1996).

In this paper, we present spherical thin-plate models focusing on the Amurian continental plate using the finite-element code SHELLS developed by Bird (1999). This 2-D modelling code simulates short-term deformation and kinematics of a two-layered lithosphere with lateral variations of crustal and lithospheric thicknesses. We first define the Amurian Plate, discuss its geometry and analyse its kinematics and deformation through published GPS and seismotectonic data (Parfenov *et al.* 1987; Petit *et al.* 1996; Wei & Seno 1998; Heki *et al.* 1999; Wang *et al.* 2001; Calais *et al.* 2003; Reinecker *et al.* 2003; Dziewonski *et al.* 2003, and references therein). Then, we present results of forward modelling which allow evaluation of the role of body and boundary forces in the deformation of the Amurian domain.

In a similar approach, Polyansky (2002) used the SHELLS finite-element code to reproduce the velocity and stress fields of the Baikal Rift region. They have shown that a combination of northeast-directed compression and southeast extension can explain the local velocity and stress fields. Our regional study is complementary to theirs which focuses on the Baikal Rift dynamics in a purely intraplate context.

2 IS THERE AN AMURIAN PLATE?

Accurate definition of plate geometries within deforming continents is difficult because deformation can be very slow and spread over a wide area, so that it might be difficult to discriminate 'rigid' plate domains from deforming ones. Several types of data help distinguish plate-like behaviour of continental domains and define their boundaries:

(1) Seismicity distribution gives a snapshot of the present-day brittle deformation. In addition to simple epicentre maps, computation of the seismic moment release has proved useful in delineating areas of high strain rates (e.g. Molnar & Deng 1984; Holt *et al.* 1995; Kreemer *et al.* 2003). However, the very short time span of seismic catalogues with respect to the seismic cycle (especially in slowly deforming regions like northeast Asia) limits the accuracy of this method. Indeed, the deformation imaged by seismic moment maps will depend on complex interactions between far-field loading, fault mechanical behaviour and fault interactions. For example, four earthquakes of magnitude greater than 8 occurred in Mongolia during the first half of the 20th century, releasing most of the accumulated elastic deformation of the whole of Asia during this time span (e.g. Baljinnyam *et al.* 1993); this is in contradiction to the low recent fault rates and GPS velocities (Ritz *et al.* 1995; Calais *et al.* 2003). Hence, except for peculiar cases (large seismic catalogue, rapidly deforming areas), maps of seismic moment release have to be interpreted carefully.

(2) Geodetic data can be used to define 'stable' plate interiors matching rigid rotation models within a certain amount of uncertainty. These types of data are much less dependent upon the fault behaviour than seismicity; on the other hand, acceptable misfits for GPS-derived rigid rotations (typically $\sim$1–2 mm yr^{-1}) might have non-negligible effects on deformations over geological time.

This problem of plate definition is still debated in northeast Asia, around the Amurian region (Fig. 1). While most authors agree to define an extruding East Asian domain composed of Amuria, North China, South China and Sundaland 'rigid' blocks, there is no clear definition of their common boundary geometries and kinematics. Among them, Amuria (AM) is the northernmost continental domain extruded eastward in response to the India–Asia collision (Fig. 1). The Baikal Rift system and the Stanovoy range represent its western and northern boundaries with the Siberian Craton which pertains to the Eurasian Plate (EU). To the east, the Sakhalin and Japan deforming zones separate it from the Okhotsk (OK) or North America (NA) and Philippine Sea (PHS) plates (e.g. Seno *et al.* 1996). In the rest of the paper, we will use capital letters (e.g. OK/AM) to designate relative plate velocities and small letters (e.g. am/eu) to indicate plate boundaries. The Philippine Sea Plate is subducting beneath Amuria along southwest Japan, while incipient eastward subduction of the Sea of Japan beneath the Okhotsk Plate has been evidenced northwards (e.g. Nakamura 1983; Tamaki & Honza 1984; Sagiya *et al.* 2000). Finally, OK/AM relative motion in Sakhalin results in dextral transpression along major north–south trending faults (Fournier *et al.* 1994; Weaver *et al.* 2003). The southern boundary of Amuria is more difficult to draw. According to the seismicity map (Fig. 1), it runs east–west at 40°N following the Hetao grabens to the north of the Ordos Block, the Gobi–Altai range and northwest up to the Altai. However, Heki *et al.* (1999) place it south of the Ordos Block and Calais *et al.* (2003) show that GPS measurements do not detect relative motions larger than 2 mm yr^{-1} between Amuria, North China and South China, making of all them a 'kinematically' rigid unique block. The region between Amuria and North China is characterized by east–west left-lateral faulting and a weak southward jump of GPS velocities (see Figs 2a and c) which suggests that the Ordos and South China domains are extruded slightly faster than the Amurian Plate (Zhang *et al.* 1998; Takahashi *et al.* 1999; Shen *et al.* 2000; Bird 2003). Also, recent global models of plate rotation and deformation result in non-negligible (although small) deformation along this same boundary (Kreemer *et al.* 2003).

In summary, the northern and eastern limits of the Amurian Plate look like 'true' plate boundaries with localized deformation; its southern limit is part of the Asian deformation domain and is less clearly localized, possibly because differential motions between Amuria and North and South China are slow and taken up over a wide deformed zone rather than being strictly localized along a single major fault. In the following models, we will use an Amurian Plate definition with a southern limit running from the Gobi–Altai to Korea and South Japan. This plate corresponds to a wide continental region where only a few earthquakes have occurred, except in western Mongolia and south of Lake Baikal where more abundant seismicity suggests intraplate deformation.

In the following section, we present stress and kinematic data around and within the Amurian Plate, which are then used as constraints to our models.

3 STRESS AND VELOCITY FIELDS OF THE AMURIAN PLATE

3.1 Kinematic and stress field data

3.1.1 Earthquake slip vectors

The use of earthquake slip vectors to determine the kinematics of continental plates has some intrinsic difficulties, because: (1) distinction between interplate and intraplate events is sometimes

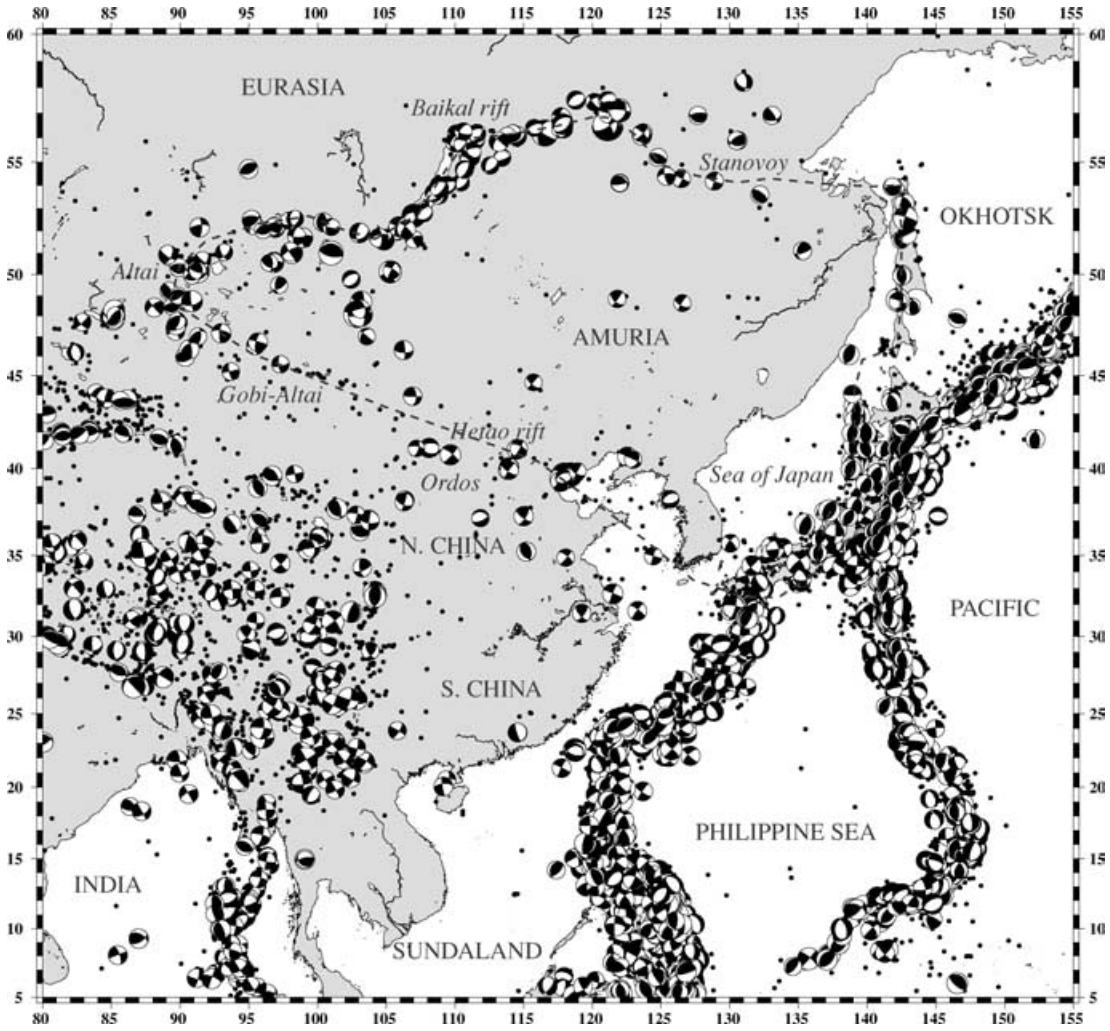

Figure 1. General setting and seismicity in eastern Asia. Epicentres come from the NEIC International Data Center (depth <50 km); focal solutions come from CMT (Dziewonski *et al.* 2003, and references therein) except for focal solutions and epicentres in the Stanovoy and Baikal regions which come from local data published in Parfenov *et al.* (1987) and Petit *et al.* (1996). The broken line indicates the inferred boundaries of the Amurian Plate.

ambiguous; (2) without accurate knowledge of the fault orientation, selection of the actual fault plane and slip vector is difficult, and (3) given the complex geometry of plate boundaries in continental domains, earthquake slip vectors may not trend strictly parallel to the direction of plate motion (e.g. Jestin *et al.* 1994). However, it remains a useful and reliable database in places where no other kinematic data exist. Up to now, a large part of the Amurian Plate has remained uncovered by GPS measurements. This is especially true along its northeastern plate boundary, i.e. in the North Baikal and Stanovoy regions. Kinematic data on these deforming zones are of crucial interest to better understand the Amurian Plate motion and deformations, and to constrain any mechanical model. We therefore use earthquake data (slip vectors and stress field) in order to overcome the lack of GPS data in the north and bring additional constraints (stress regime) in regions covered by GPS (Fig. 2a).

We compile focal mechanism data around the Amurian Plate using different databases (Figs 1 and 2a): Harvard CMT solutions (Dziewonski *et al.* 2003, and references therein) for Japan, North China and Mongolia regions and first-motion local determinations for earthquakes of the Baikal Rift (Petit *et al.* 1996) and Stanovoy range (Parfenov *et al.* 1987). Fig. 2(a) shows slip vectors of the focal solutions presented in Fig. 1. Fault planes and associated slip vectors are chosen according to their consistency with known fault directions (Baikal, Stanovoy, Mongolia) and slab dip angle (Japan subductions). Solutions with ambiguous fault plane determinations are rejected. Earthquake slip vectors show constant trends along the phs/am and ok/am plate boundaries. On the contrary, slip vector azimuths differ by about 80° between North Baikal and Stanovoy areas, reflecting a transition from northwest–southeast extension to northeast–southwest compression. In western Mongolia, mixed approximately northwest–southeast and east–west directions reflect the complex interference between dextral motions along the north–south active faults of Altai and left-lateral strike-slip faulting along the east–west faults of central Mongolia. Finally, left-lateral east–west motions north of the North China grabens are in agreement with the velocity gradient between Amuria and Ordos.

Slip vectors are kinematic indicators of the relative motion of Amuria with respect to adjacent plates. They cannot be compared directly with GPS data or even with the modelled velocities which are all represented with respect to Eurasia, except along the Baikal–Stanovoy boundary where slip vectors do correspond to AM/EU motion. Hence, they can be used for constraining modelled velocities along the AM/EU boundary and, if needed, for determining the

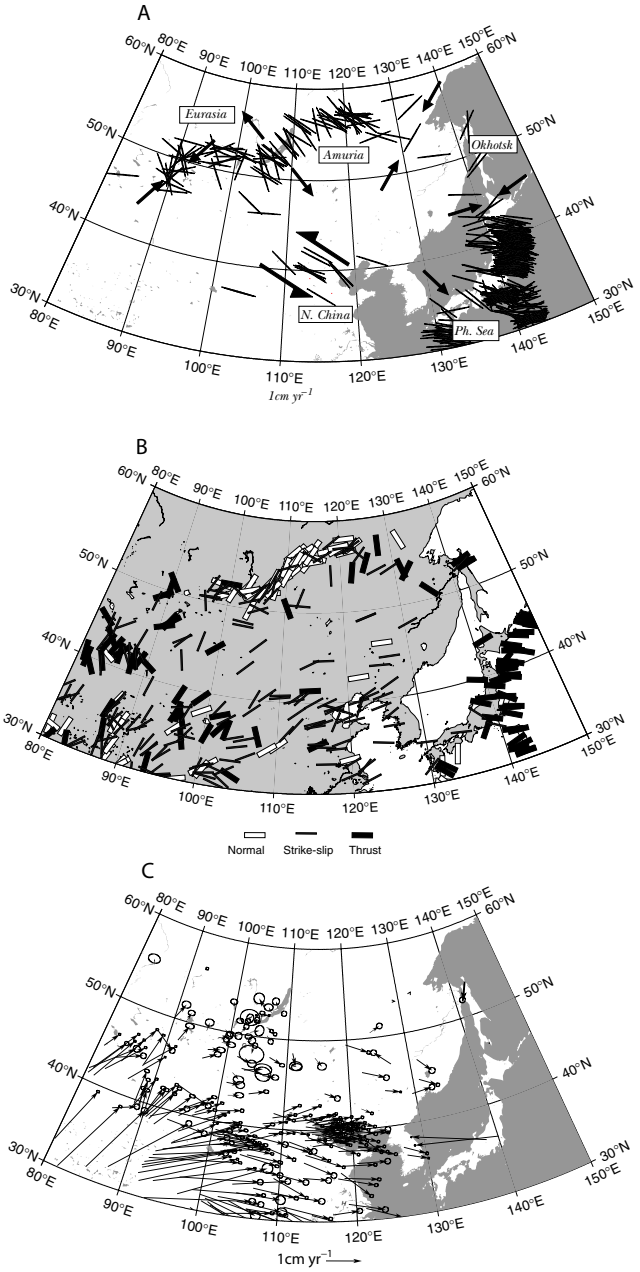

Figure 2. Stress field and velocities in and around the Amurian Plate from earthquake and GPS data. (A) Earthquake slip vectors (thin lines) inferred from CMT and local fault plane solutions (see Fig. 1). Arrows indicate directions of relative plate motions. (B) Maximum horizontal stress ($\sigma h_{\max}$) directions from the World Stress Map, after Reinecker *et al.* (2003). (C) GPS vectors with respect to Eurasia in the ITRF2000 reference frame, after Calais *et al.* (2003) (Baikal–Mongolia), Wang *et al.* (2001) (China) and Heki *et al.* (1999) (Sakhalin).

azimuth of the relative motion of adjacent plates with respect to Amuria.

3.1.2 Amurian Plate stress field

Stress field data for the Amurian Plate mainly come from focal mechanisms of earthquakes (Reinecker *et al.* 2003). These data consist of *P* or *N* principal axes of deformation, which are not 'true' principal stress axes σ_1 or σ_2. In a given region, provided *P* and *N* axes correspond to different types of focal solutions, their mean direction can be taken as representative of the mean maximum horizontal stress direction $\sigma h_{\max}$ (Zoback 1992). The Amurian Plate experiences different stress regimes and directions along its boundaries, going from pure northwest–southeast extension in the Baikal Rift to pure approximately east–west compression on the eastern margin of the Sea of Japan (Fig. 2b). The stress field is dominantly strike-slip along its southern boundary (except in western Mongolia where compressional stress regimes are observed) and rapidly changes from northwest–southeast extension to north–south compression along its northern boundary.

3.1.3 GPS data

In this study, we use as velocity constraints in our models the recent GPS data published by Wang *et al.* (2001) and Calais *et al.* (2003) for the China, Mongolia and Baikal regions (Fig. 2c). We add to this data set the velocity of the OKHA station in northern Sakhalin (Heki *et al.* 1999). In order to have a consistent view of the velocity field over the Amurian Plate, all velocity vectors are plotted in an ITRF2000 (international terrestrial reference frame), Eurasia-fixed reference frame (Fig. 2c).

GPS data depict different motions along the boundaries of the Amurian Plate: on the southern boundary, velocities between longitudes 90°E and 100°E are relatively low (∼5 mm yr^{-1}) and their azimuths rapidly change from ∼N20 to ∼N90. East of longitude 100°E, velocities rapidly increase to about 6 to 8 mm yr^{-1} in a constant ∼N110 direction. Along the Baikal Rift, northwest–southeast extension dominates at rates of about 4 mm yr^{-1}.

3.2 Rigid-rotation models of the Amurian Plate motion

No fewer than six different Euler rotation poles for the Amuria/Eurasia motion have been proposed up to now. We compare these solutions in the light of kinematic and stress data. Fig. 3 shows the small circles centred on the AM/EU rotation pole of each solution. Based on inversion of slip vectors of earthquakes in the Baikal and Stanovoy areas, Zonenshain & Savostin (1981) and Wei & Seno (1998) found a AM/EU pole located close to the northern Amurian Plate boundary, the latter being in good agreement with observed kinematics and stress fields. The pole of Wei & Seno (1998) satisfyingly reproduces observed displacements along Baikal, Stanovoy, and North Ordos.

Recently, Calais *et al.* (2003) determined GPS velocities in the Baikal Rift and Mongolia regions with respect to a stable Eurasia. They show a west–east transition from dominantly northward to eastward motions at ∼4–5 mm yr^{-1} in western Mongolia, changing to approximately northwest–southeast opening in the Baikal Rift at a rate of about 3–4 mm yr^{-1}. From these GPS data and those of Wang *et al.* (2001), Calais *et al.* (2003) determined an AM/EU rotation pole located north of the Stanovoy range at about 62°N, 135°E. This solution, obtained with a different data set, is in good agreement with the solution of Wei & Seno (1998). Both poles satisfy observed motions except in Sakhalin, around the Sea of Japan and in western Mongolia.

Heki *et al.* (1999) determined the Euler vector between the Amurian and Eurasian plates from five GPS station velocities and found a AM/EU rotation pole located at 22.3°S, 106.6°E, with a rotation rate of −0.091° Myr^{-1}. The discrepancy between their solution and others partly comes from the use of different realizations of stable Eurasia (e.g. Calais & Amarjargal 2000). Indeed, Heki *et al.* (1999) used the NUVEL1-NNR model to define stable

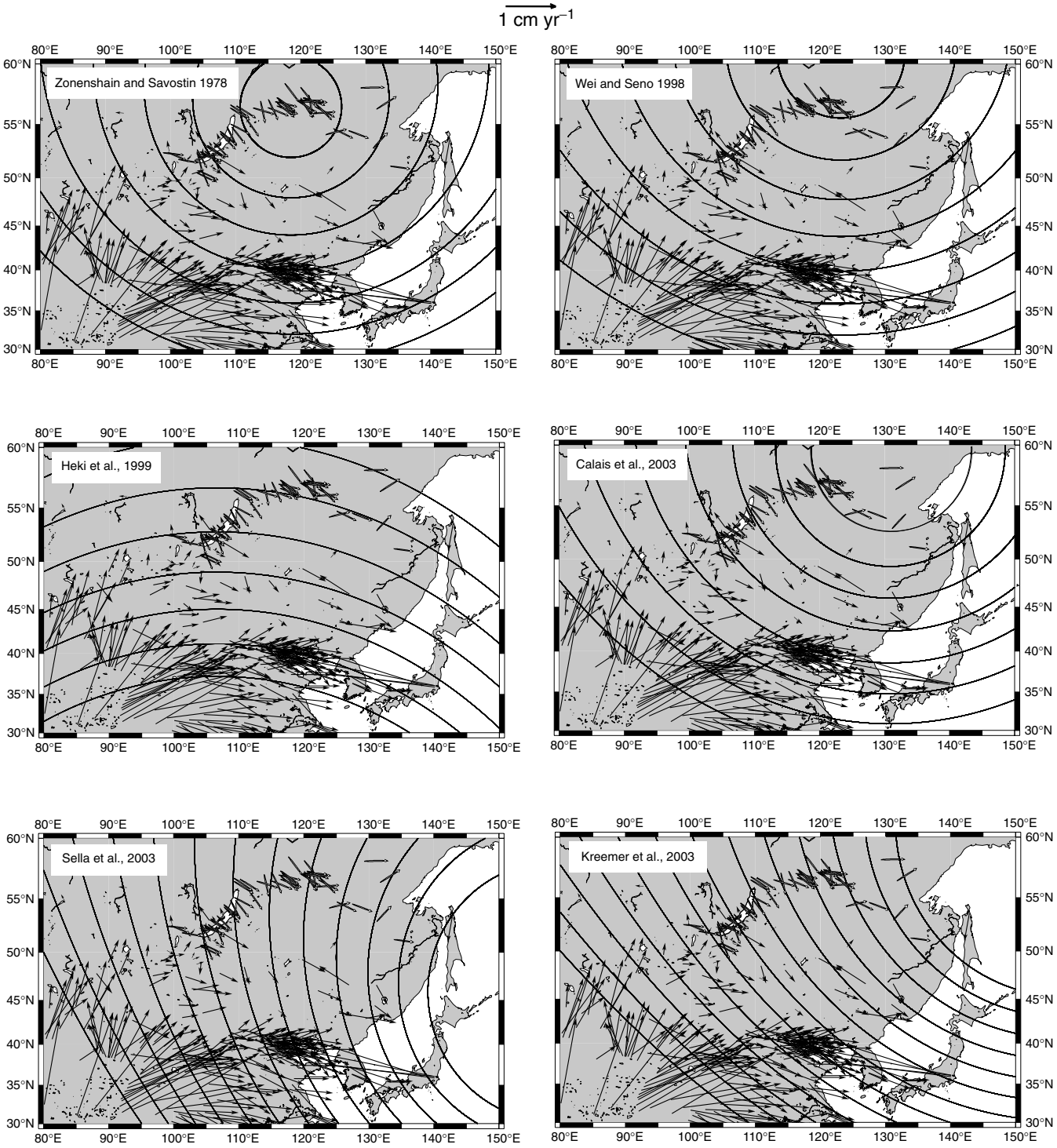

Figure 3. Comparison of GPS and slip vector data with rigid rotation models of AM/EU proposed by different authors: small circles correspond to published AM/EU rotation poles; open arrows are earthquake slip vectors along the Baikal–Stanovoy boundary; solid arrows are GPS velocities (see Fig. 2).

Eurasia, which leads to an exaggeration of the eastward motion of Amuria but does not strongly change vector azimuths. In any case, their pole is in good agreement with GPS vectors located in the southeastern domain of the plate domain but predict inconsistent motions and stress fields elsewhere. Indeed, clockwise rotation of Amuria around the pole proposed by Heki *et al.* (1999) results in rapid, strike-slip to oblique extensional motions all along Baikal and Stanovoy, which are not observed.

Finally, recent global kinematic models based on GPS data like REVEL (Sella *et al.* 2002) and GRSM (Kreemer *et al.* 2003) have proposed different AM/EU rotation poles. Surprisingly, both of them find a pole located east of Amuria, resulting in north–south to northwest–southeast extension along almost all the am/eu boundary, which is again not in agreement with data. Clearly, as pointed out by Kreemer *et al.* (2003), the AM/EU rotation is not well constrained by global kinematic models.

In summary, some rigid rotation models like those of Wei & Seno (1998) and Calais *et al.* (2003) are in good agreement with an important number of geodetic and seismological data. However, significant misfits remain, especially around Mongolia and the Sea of Japan, suggesting intraplate deformation. In the following sections we try to clarify this by testing the influence of body and boundary forces on the velocity and stress fields. GPS and stress data located around the plate are used as *a priori* constraints on the model, while *a posteriori* constraints are given by intraplate data.

4 MODELLING THE AMURIAN PLATE KINEMATICS

4.1 Modelling procedure

SHELLS is a spherical 2-D finite-element code which allows handling of a two-layered lithosphere with different rheological properties in the crust and mantle. Rheological layering involves frictional sliding for the upper, resistant parts of the crust and mantle lithosphere and non-linear viscous creep for ductile domains (Bird 1999). The study area is divided into triangular elements of arbitrary dimensions. Faults with various dips can be introduced in the model, following element boundaries, so that faulted nodes are split into two nodes which can move with respect to each other. The model outputs velocity and stress fields as well as fault slip rates.

A comprehensive description of the model's governing equations can be found in Bird (1999) and an application to Baikal Rift dynamics is presented in Polyansky (2002). We briefly recall here its principal aspects. The model uses the Boussinesq approximation of incompressibility in the mass conservation equation. Elastic strain is neglected in the model, so that output displacements must be interpreted as an average over a time span longer than the seismic cycle. The force balance is obtained by integrating vertically the horizontal components of moment, since it is assumed that horizontal velocity does not vary significantly with depth. The horizontal components of the stress tensor are also integrated over depth. The thermal part of the model uses vertical heat transfer with constant thermal properties in the crust and mantle. It does not take into account advection, lateral heat transfer or viscous heat dissipation.

The lithosphere has two brittle/ductile layers corresponding to the crust and upper mantle. The grid is one element thick; thus one grid element has the integrated strength of both its crust and mantle parts.

Brittle rheology is defined by the Mohr–Coulomb criterion, with the friction coefficient f being different on the fault surface than within continuous elements (Table 1):

$$\sigma_{\text{friction}} < f(-\sigma_{\text{n}} - BiPp) + \sigma_{\text{c}} \tag{1}$$

Table 1. Physical lithospheric parameters used in the modelling.

Parameter	Crust	Mantle
Density, ρ (kg m^{-3})	2800	3332
Continuum friction coefficient	0.85	
Biot coefficient, *Bi*	1.0	
Thermal conductivity, K (W m^{-1} K^{-1})	3.0	4.0
Radioactive heat production, H (W m^{-3})	4.5×10^{-7}	3.2×10^{-8}
ACREEP (Pa s$^{1/n}$)	2.3×10^{9}	5.3×10^{5}
BCREEP (K)	4000	18 314
CCREEP (K Pa^{-1})	0	0.0171
D (maximum shear stress) (Pa)	5×10^{8}	
ECREEP	0.33333	

where σ_{n} is the normal stress, *Bi* is the Biot coefficient, *Pp* the efficacy of pore pressure and σ_{c} is the cohesion (assumed to be low on fault planes).

Ductile rheology is defined by power-law creep:

$$\sigma_{\text{creep}} = \text{ACREEP} \times \dot{E}^{\text{ECREEP}} \times \exp[(\text{BCREEP} + \text{CCREEP} \times \text{depth})/T]. \tag{2}$$

ACREEP, BCREEP and ECREEP are creep parameters of the model, whose values are given in Table 1, $\dot{E}$ is the strain rate and T is temperature in kelvin. Equivalence with classical power-law creep parameters is as follows:

$$\text{ACREEP} = 1/A^*$$
$$\text{BCREEP} = E^*/nR$$
$$\text{ECREEP} = 1/n$$
$$\text{CCREEP} = Va/nR$$

with A^* the pre-exponential creep parameter, E^* the activation energy, *Va* the activation volume and n the power-law exponent. We used olivine-dominated (dunite) rheology for the continental mantle and quartz-diorite-dominated rheology for the continental crust. Temperature at a given depth z is computed from surface heat flow data using:

$$T_n(z) = T_0 + \frac{(Q_{\text{b}} + h_n H_n)(z - z_t)}{K_n} - \frac{H_n(z - z_t)^2}{2K_n} \tag{3}$$

with T_0 the surface temperature, z_t the surface coordinate of layer n, $Q_{\text{s}} = Q_{\text{b}} + h_n H_n$ the surface heat flow (background flow and radioactive heat production), K_n the thermal conductivity and H_n the radioactive heat production per volume unit of layer n ($n = 1$ for the crust, $n = 2$ for the mantle).

4.2 Initial parameters

4.2.1 Mesh and faults

The plate is represented by 327 triangular elements of varying sizes, with higher resolution along the Baikal Rift where GPS, earthquake data and fault geometries are best documented (Fig. 4a). When faulted elements are located on the perimeter of the model, applied boundary conditions are those of the adjacent plates (see Section 4.2.3). For the Amurian Plate, far-field stresses mainly come from the India–Asia collision and are responsible for observed velocities along the southern model boundary. Thus, nodes located on this boundary should pertain to the Amurian Plate and we left them unfaulted. Normal faults with high dip (60°) run along the Baikal Rift and define the northwestern am/eu plate boundary. To the northeast, in the Stanovoy range, this limit is defined by vertical faults trending approximately east–west. Subduction of the Philippine Sea Plate along southwest Japan is simulated by a westward low-dipping (30°) fault plane which joins the eastward-dipping subduction of the Sea of Japan through a vertical transfer zone (the Itoigawa–Shizuoka tectonic line). Along Sakhalin Island, the ok/am boundary is represented by an approximately north–south wrench-reverse fault. Friction on fault planes is low (0.03). The value of the fault friction coefficient determines whether the deformation due to the relative motion of these plates is transmitted—'diffused'—within the plate interior or localized along faulted boundaries. With higher fault friction coefficients faults do not move and the deformation is essentially diffused within the plate interior. One must notice that model faults cut out through the whole lithosphere, since the grid is only one node thick. Hence, slip along these deep faults requires either huge stresses or low friction.

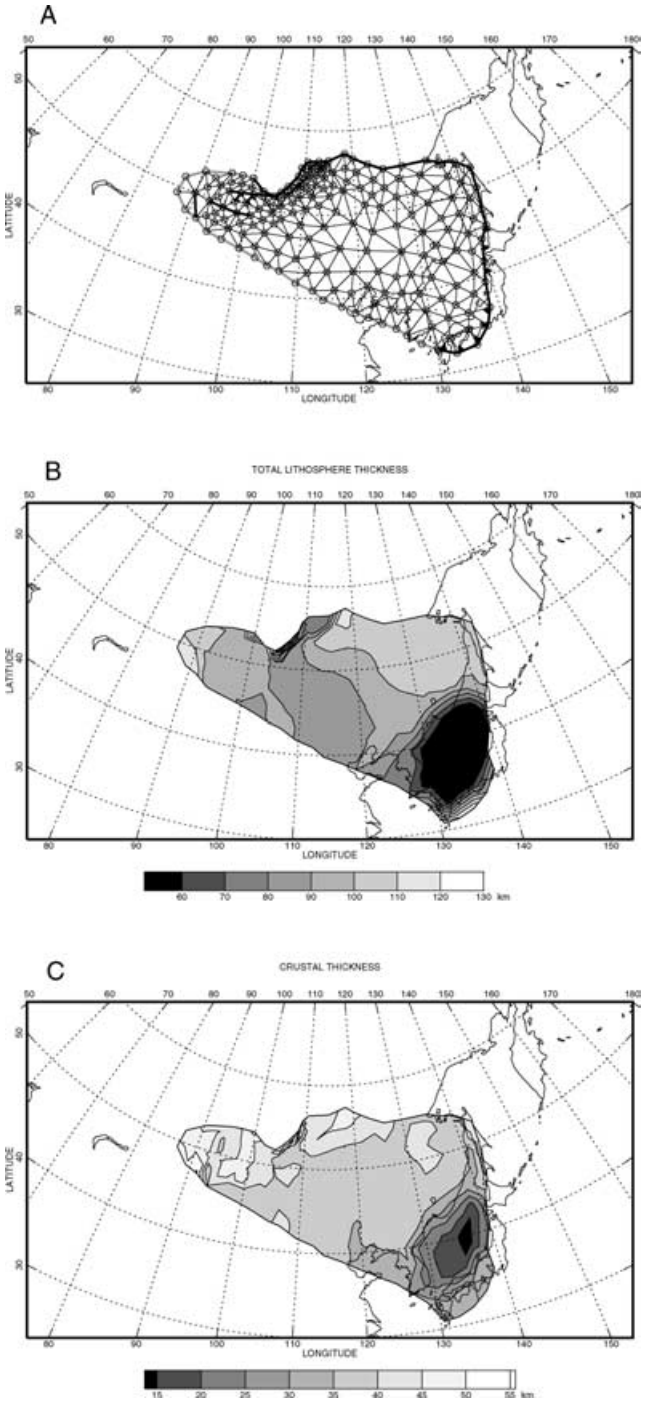

Figure 4. Finite-element grid of the Amurian Plate. (A) Finite-element and fault (thick lines) geometries. (B) Thickness of the mantle lithosphere, taken as the depth of the 1300 °C isotherm computed from heat flow values (Pollack *et al.* 1993; Lysak 1992). (C) Thickness of the crust, computed from GTOPO30 topography data and assuming local isostasy (*cf.* Table 1).

4.2.2 Lithospheric structure

Surface topography is derived from the worldwide GTOPO30 database. Heat flow comes from the worldwide Global Heat Flow Database compilation (http://www.heatflow.und.edu) by Pollack *et al.* (1993). In this database, heat flow measurements for the Baikal region come from the study of Lysak (1992). Crust and mantle lithosphere thicknesses are computed to achieve local isostasy at any point of the model (Figs 4b and c). Lithosphere thickness is computed from heat flow values as the depth of the 1300 °C isotherm. The resulting total lithospheric thickness is highest (>100 km) in the north of the grid which is located within the Aldan Shield (Siberian Craton). Thin lithosphere is encountered in the Sea of Japan. Note that, due to the relatively low heat flow value, the lithosphere is not significantly thinner in the Baikal Rift than in surrounding regions. Crustal thickness ranges between ∼15 km in the Sea of Japan (simulating oceanic crust) and >50 km in the highest ranges of Mongolia.

4.2.3 Velocity conditions

We tested 23 models based on different velocity conditions applied at the grid boundaries (Fig. 5, Table 2). Applied boundary conditions are of three types:

(1) The so-called 'free' boundary condition refers to applied lithostatic normal traction only and is achieved by assuming an adjacent lithospheric column of identical thickness (same lithostatic pressure) and of infinitely low strength.

(2) 2-D velocity conditions for internal (i.e. unfaulted) boundary nodes consist of fixed azimuths and displacement rates, so that the two components of the velocity vectors are imposed (i.e. zero degrees of freedom).

(3) 2-D velocity conditions for external (i.e. faulted) boundary nodes consist of fixed azimuths and velocities of adjacent plates. Shear and normal traction exerted on the fault are linearly related to node relative velocities on both sides of the fault, depending on its friction coefficient. Hence, perimeter faults have boundary conditions similar to frictional boundaries.

In all the models, a stable Eurasia is obtained by applying null velocities on the 'outside' boundary elements located from the Sayan range west of Lake Baikal to the eastern end of the Stanovoy range (Fig. 5). We first test the influence of body forces by applying only lithostatic normal traction (hereafter referred to as the 'free' boundary condition) to all boundary elements except these (model 1). Then we test the role of 'collision–extrusion' processes by adding northeast to east-southeast- trending velocity vectors at rates of 6 to 8 mm yr^{-1} along the southern boundary, based on GPS data, the eastern boundary remaining free (model 2). Finally, we examine the role of Pacific (*sensu lato*) subductions by testing different PHS/EU and OK/EU rates of convergence based on the REVEL (Sella *et al.* 2002) global kinematic model.

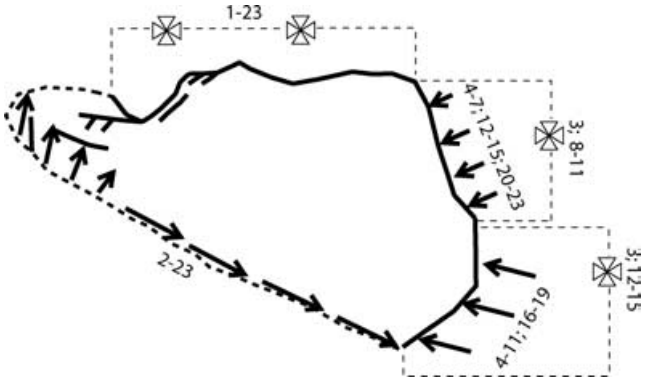

Figure 5. Synthesis of boundary conditions for the 23 tested models: open cross, fixed boundary (i.e. null velocity with respect to Eurasia); solid arrows, non-null 2-D velocity conditions. Outside/inside arrows mean that 2-D velocity conditions apply to external/internal nodes, respectively. If nothing is specified, boundary nodes are left free (see explanations in the text).

Table 2. Tested velocity conditions on the boundaries of the Amurian Plate. PHS/EU and OK/EU vectors have been determined using the REVEL (Sella *et al.* 2002) global kinematic model.

Model	South	NW	East (PHS)	East (OK)
1	Free	Fixed	Free	Free
2	NE to SE motion	Fixed	Free	Free
3	NE to SE motion	Fixed	Fixed	Fixed
4	NE to SE motion	Fixed	PHS/EU 1/4 motion	OK/EU 1/4 motion
5	NE to SE motion	Fixed	PHS/EU 1/2 motion	OK/EU 1/2 motion
6	NE to SE motion	Fixed	PHS/EU 3/4 motion	OK/EU 3/4 motion
7	NE to SE motion	Fixed	PHS/EU full motion	OK/EU full motion
8	NE to SE motion	Fixed	PHS/EU 1/4 motion	Fixed
9	NE to SE motion	Fixed	PHS/EU 1/2 motion	Fixed
10	NE to SE motion	Fixed	PHS/EU 3/4 motion	Fixed
11	NE to SE motion	Fixed	PHS/EU full motion	Fixed
12	NE to SE motion	Fixed	Fixed	OK/EU 1/4 motion
13	NE to SE motion	Fixed	Fixed	OK/EU 1/2 motion
14	NE to SE motion	Fixed	Fixed	OK/EU 3/4 motion
15	NE to SE motion	Fixed	Fixed	OK/EU full motion
16	NE to SE motion	Fixed	PHS/EU 1/4 motion	Free
17	NE to SE motion	Fixed	PHS/EU 1/2 motion	Free
18	NE to SE motion	Fixed	PHS/EU 3/4 motion	Free
19	NE to SE motion	Fixed	PHS/EU full motion	Free
20	NE to SE motion	Fixed	Free	OK/EU 1/4 motion
21	NE to SE motion	Fixed	Free	OK/EU 1/2 motion
22	NE to SE motion	Fixed	Free	OK/EU 3/4 motion
23	NE to SE motion	Fixed	Free	OK/EU full motion

Table 3. Misfit (RMS residuals) of the different models with respect to GPS, slip vectors and stress data (model numbers refer to Table 1). Ouput velocities and stresses are compared with GPS measurements (column 2), slip vector azimuths on the Baikal–Stanovoy boundary (column 3), σh_{max} azimuth (column 4) and stress regimes. Column 5 indicates the percentage of bad regimes output by the models, compared with World Stress Map (WSM) data and column 6 ranks the models.

Model	GPS data RMS (mm yr^{-1})	Slip vector azimuth RMS (°)	Stress data		Rank[a]
			Azimuth RMS (°)	Bad regimes (per cent)	
1	4.4	65	45.5	65	D
2	4.0	23	37.6	44	B
3	**3.8**	**25**	**30.7**	**45**	**A**
4	3.6	39	34.3	45	C
5	3.7	40	38.8	52	D
6	4.2	37	41.5	58	D
7	5.0	44	42.2	60	D
8	3.6	31	31.2	45	B
9	3.5	50	31.2	48	D
10	4.0	32	31.2	48	B
11	4.7	33	31.1	48	C
12	3.9	33	32.3	44	B
13	3.9	37	36.2	47	C
14	3.9	52	37.9	50	D
15	4.0	46	40.0	54	D
16	**3.6**	**24**	**32.9**	**44**	**A**
17	**3.5**	**25**	**32.9**	**44**	**A**
18	3.9	25	32.9	44	B
19	4.6	25	32.8	44	C
20	4.0	30	32.0	44	B
21	4.0	38	34.7	44	B
22	4.0	43	36.7	45	C
23	4.0	55	38.3	47	D

[a]Rank is according to the following criteria: A, GPS RMS $\leq$3.8 mm yr^{-1}, slip vector RMS $\leq$25°, σh_{max} azimuth RMS $\leq$35°, bad regimes $\leq$45 per cent; B, GPS RMS $\leq$4.2 mm yr^{-1}, slip vector RMS $\leq$35°, σh_{max} azimuth $\leq$40°, bad regimes $\leq$48 per cent; C, GPS RMS $\leq$4.8 mm yr^{-1}, slip vector RMS $\leq$45°, σh_{max} azimuth $\leq$45°, bad regimes $\leq$50 per cent; D, others. Best-fitting models are shown in bold type.

We first consider coupled PHS/EU and OK/EU convergence (models 3 to 7), then we test separately the effect of PHS/EU and OK/EU convergence, the other boundary being fixed (i.e. no relative motion with respect to Eurasia in boundary condition 3, *cf.* models 8 to 15) or free (models 16 to 23). RMS (root mean square) residuals on GPS, slip vectors and stress field data were computed for each model and are presented in Table 3. The adequacy of the results with respect to stress data is evaluated following two criteria: the adequacy of the output stress regime (extensional, compressional or strike-slip) with World Stress Map data (where a 'bad' regime means an incorrect stress regime, regardless of stress orientations) and the average angle between predicted and observed maximum horizontal stress directions (regardless of the stress regime). RMS for GPS data is computed taking into account separately the adequacy to northward and eastward components of the velocity vectors. For the sake of simplicity we only show five models in Figs 6 to 10.

4.3 Tests with body forces (model 1)

We first test the influence of body forces due to crust thickness variations (model 1, Fig. 6). The gravitational potential energy coming from thickened crust in western Mongolia appears to be the major source of body forces. Because the outside of the northern boundary of the plate does not move, only low strike-slip and compressional motions occur along the Baikal–Stanovoy region. Free boundary conditions along the southern, western and eastern limits allow for more rapid north and northeast motions, respectively. However, predicted velocities are still low (i.e. $\sim$1 mm yr^{-1} or less, except in Mongolia) and are generally not in agreement with observed ones. The predicted stress field is dominantly compressional, also because the northern plate limit is stable, and shows no resemblance to the observed one except in western Mongolia and eastern Stanovoy where approximately southwest–northeast compression is produced. This first test shows that body forces can cause only small velocities, and stress and velocity directions are generally not in agreement with the data, except in western Mongolia and Stanovoy.

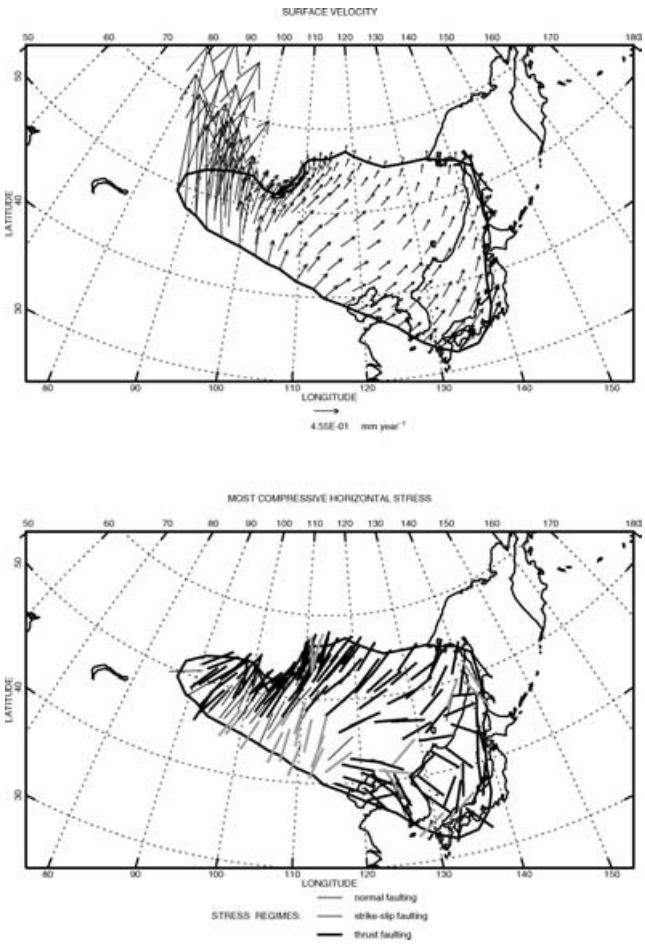

Figure 6. Velocities with respect to Eurasia (top) and stress field, represented by $\sigma h_{\max}$ directions (bottom) and for model 1.

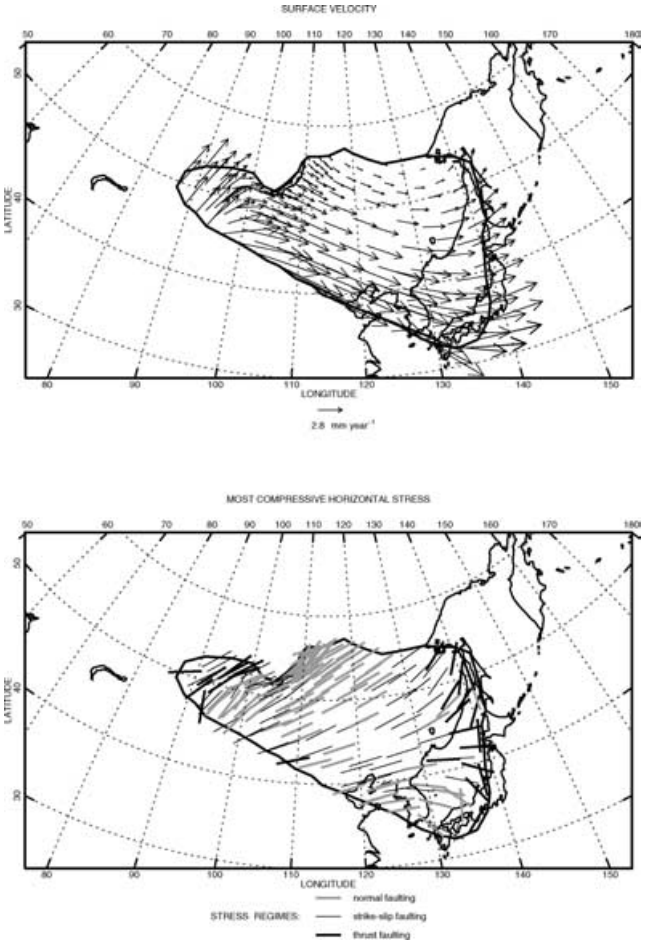

Figure 7. Same as Fig. 6 for model 2.

4.4 Tests with northeast to southeast motions along the southern boundary (model 2)

In this second test we add as boundary conditions velocities of 6 to 8 mm yr^{-1} along the southern boundary of the plate in a northeast (western Mongolia) to southeast (North China) direction (Fig. 7). The eastern plate boundary is free. Rates and azimuths are adjusted to find the best fit with stress and GPS data along the southern boundary. This model satisfyingly reproduces the observed northeast–southwest extension in the Baikal region, as well and northwest–southeast compression in western Mongolia. The transition from extension to compression in North Baikal–Stanovoy is also well predicted, but occurs more eastwards than observed on the stress field map (Fig. 2). Predicted velocities in the Baikal Rift and Mongolia are of about 2–3 mm yr^{-1}, which is close to observations (Calais *et al.* 2003; Vergnolle & Calais 2003). On the other hand, the

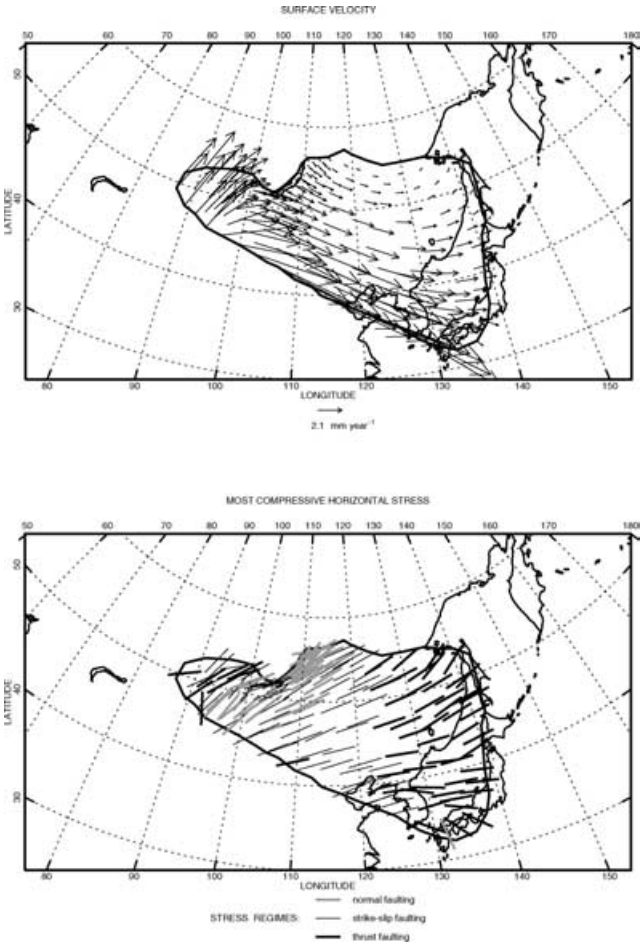

Figure 8. Same as Fig. 6 for model 3.

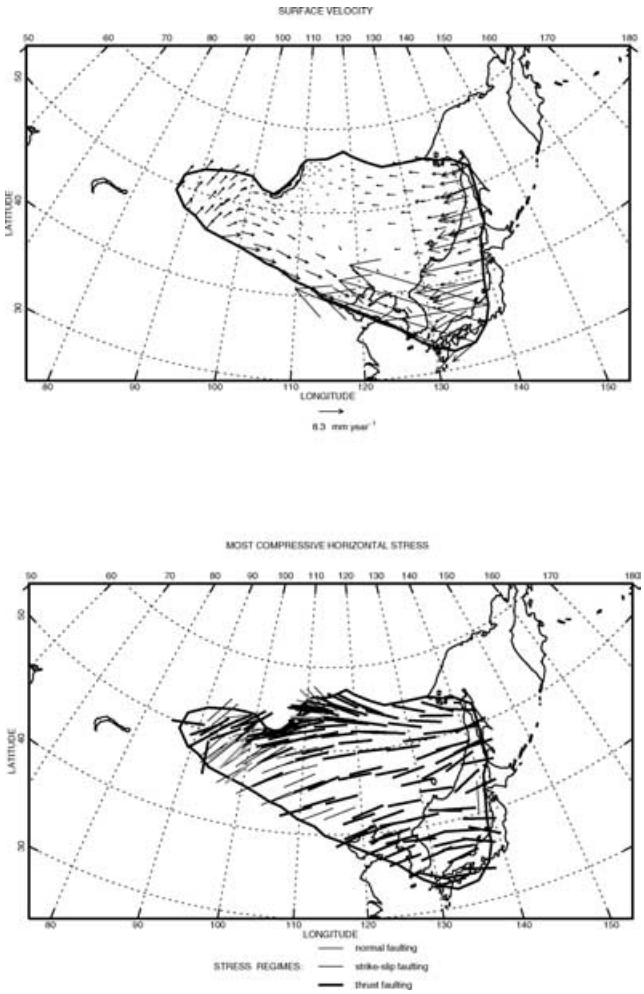

Figure 9. Same as Fig. 6 for model 7.

model predicts extensional stress regime south of the Baikal Rift, in Korea and South Japan, which is not observed. In addition, modelled velocities and stress fields along the boundary of the eastern plate do not match the data, suggesting that the free boundary condition is not a relevant approximation for this limit.

4.5 Tests with velocity conditions along the Philippine Sea and Okhotsk plate margins (models 3 to 23)

In the third set of experiments, we test the influence of East Asian subduction by adding variable rates of plate convergence along the southeastern plate limit (i.e. southwest Japan), based on relative PHS/EU azimuths and rates calculated from REVEL (Sella *et al.* 2002). The problem is to know what amount of stress due to plate convergence is transferred into the interior of the Amurian Plate. We first tested coupled OK/EU and PHS/EU convergence with velocities of 0 (i.e. no relative OK/EU and PHS/EU motion), 25, 50, 75 and 100 per cent of their REVEL rate (models 3 to 7). As the fault friction coefficient is kept constant for all the experiments, the amount of stress transfer depends on the applied velocity vector. Misfit tests (Table 3) show that the best results are found for model 3, i.e. with null OK/EU and PHS/EU relative motion. This model predicts compression in the southeastern part of the plate, and a domain of strike-slip regime in its centre, which is in good agreement with stress field data (Fig. 8). Stress regimes and directions are also well reproduced in the Baikal region, with a dominant strike-slip regime in South Baikal, changing to extension in the central and northern rift zones. Extension dominates south of the Baikal Rift, which is not observed except in the north–south grabens of northwestern Mongolia. Rapid change from extension to compression in the north occurs at a longitude of ∼125°E, which is very close to observations as well. The model also fits the observed dominant southwest–northeast compression in southwestern Mongolia, progressively changing to a strike-slip regime with $\sigma 1$ trending west-southwest to east-northeast along the Gobi–Altai and North China regions. Predicted velocities of ∼2–3 mm yr^{-1} in the southern Baikal Rift and Mongolia are similar to those found in model 2, because what happens on the eastern boundary does not strongly affect the western part of the plate. Model 3 also better fits stress and GPS directions than model 2 (free eastern boundary), which means that a frictional eastern boundary weakly resisting the Amurian extrusion is more relevant than a 'free' one.

Increasing the amount of relative convergence with coupled plates yields larger misfits, especially for stress field data, because of the transfer of compressional stresses far into the plate interior. Fig. 9 shows the results of model 7, i.e. with 100 per cent of the REVEL OK/EU and PHS/EU convergence rates. Despite the low fault friction coefficient, east–west compression is transmitted over the whole plate, even in the Baikal Rift. The model predicts right lateral motions along the North Baikal–Stanovoy boundary, oppositely to observed ones.

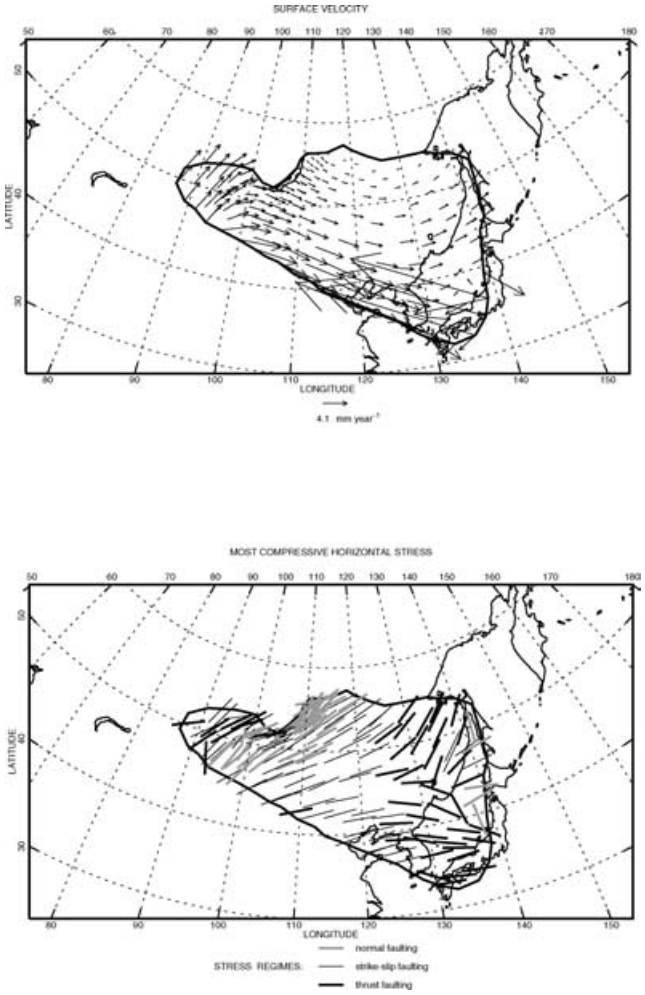

Figure 10. Same as Fig. 6 for model 16.

Then, we tested separately the influence of OK/EU and PHS/EU convergence. When one boundary is fixed (i.e. zero OK/EU or PHS/EU relative motion), increasing the convergence rate of the other plate increases the misfit (Table 3, models 8 to 15). Hence for the set of models 3 to 15, the best one is for null OK/EU and PHS/EU velocities (model 3). When the other the OK/EU or PHS/EU boundary is left free, increasing the amount of relative convergence of the other plate has less dramatic effects on the goodness of fit (Table 3, models 16 to 23). This set of experiments shows that good fits are found for moving PHS/EU at 25 or 50 per cent of its REVEL rate, and free OK/EU (models 16 and 17).

In summary, misfit tests do not allow us to discriminate between model 3 and models 16 or 17. Comparison of Figs 8 and 10 gives a better understanding of the differences between these models (here, models 3 and 16). Both predict similar velocities and stresses in the western part of the plate, but show significant differences in the eastern part: while a rather smooth compressional stress field is predicted by model 3 from Stanovoy to South Korea, model 16 shows abrupt changes in stress directions and regimes, with east–west to north–south extension in some places near Sakhalin and the northern Sea of Japan. Misfit tests are not sensitive to these differences, mainly because there are very few data for along Sakhalin Island (Figs 1 and 2). However, earthquake focal mechanisms and field studies bring evidence for recent transpressional dextral motions in Sakhalin (Fournier *et al.* 1994), which rather favours a fixed OK/EU velocity condition similar to model 3. In this case, observed long-term north–south dextral motions in Sakhalin, and northeast-southwest compression in South Japan would result only from AM/OK and AM/PHS convergence.

5 DISCUSSION AND CONCLUSION

Our best-fitting model (model 3, Fig. 8) shows that a west–east transition from northeast-directed compression to southeast-directed extrusion applied on the southern limit of the plate explains most of the present-day stress and velocity fields of the Amurian Plate. Northeast–southwest compression is dominant westwards, where the Amurian Plate faces the strong, undeformed Eurasia, while extrusion is allowed eastwards due to the relatively weaker Pacific boundary. Yet, the eastern plate limit does not act as a free boundary but rather as a frictional one, with a fixed adjacent plate. This would mean that, within a Eurasia-fixed reference frame, long-term compression in Sakhalin and Japan is driven by extrusion of the Amurian Plate. This is in agreement with the results of Mazzotti *et al.* (2001) and Heki & Miyazaki (2001) who show that subduction only controls the short-term (elastic) deformation in Japan.

Finally, assuming a relatively high integrated lithospheric strength, our models show that body forces play a minor role since they predict plate velocities significantly lower than those due to far-field forces. This might be the most important difference between the Amurian and other more deformed regions closer to the India indenter where over-thickened crust causes high gravitational potential energy and collapse (Bird 1991; Flesch *et al.* 2001; Fournier *et al.* 2004). One should note, however, that velocity conditions applied to the southern limit of the plate, so-called 'far-field' conditions, may themselves result from the sum of indentation, extrusion and gravitational collapse processes occurring further south.

Amongst the 'passive rifting' mechanisms responsible for the opening of the Baikal Rift about 30 Ma between Eurasia and Amuria, one could consider (1) extrusion processes coming from the south and (2) 'trench suction' along Pacific boundaries. Since the Late Miocene and up to now, the eastern limit of the Amurian Plate has undergone compression. However, before that time, the Pacific rim underwent generalized extension which caused opening of the Japan and Okhotsk seas (Jolivet *et al.* 1992; Jolivet & Tamaki 1992; Tamaki *et al.* 1992). Hence, trench suction could have helped opening of the Baikal Rift in its early stages, but is no longer a driving force in its development. Moreover, the evolution of the Baikal Rift seems characterized by an increase in the opening rate through time (e.g. Logatchev & Zorin 1987), which suggests that what occurred on the eastern plate boundary (transition from extension to compression) had little influence on it.

This seems still to be the case now, as shown by the very small difference between models 2 and 8 around Baikal. Long-lived extension in the North China grabens (Hellinger *et al.* 1985; Chen & Nabelek 1988) also seems to be little (or not) influenced by changes in tectonic regimes in Pacific subduction.

ACKNOWLEDGMENTS

We are grateful to P. Bird for providing us his modelling code SHELLS and for his generous help. Many thanks to M. Vergnolle for fruitful discussions on GPS velocities and forward modelling processes, and to two anonymous reviewers for their helpful comments.

REFERENCES

Avouac, J.-P. & Tapponnier, P., 1993. Kinematic model of active deformation in Central Asia, *Geophys. Res. Lett.,* **20,** 895–898.

Baljinnyam, I. *et al.,* 1993. *Ruptures of Major Earthquakes and Active Deformation in Mongolia and its Surroundings,* Geological Society of America Memoir 181, Geological Society of America, Boulder, CO.

Bird, P., 1991. Lateral extrusion of lower crust from under high topography in the isostatic limit, *J. geophys. Res.,* **96,** 10 275–10 286.

Bird, P., 1999. Thin-plate and thin-shell finite-element programs for forward dynamic modelling of plate deformation and faulting, *Comput. Geosci.,* **25,** 383–394.

Bird, P., 2003. An updated digital model of plate boundaries, *Geochem. Geophys. Geosyst.,* **4**(3), 1027, doi:10.1029/2001GC000252.

Calais, E. & Amarjargal, S., 2000. New constraints on current deformation in Asia from continuous GPS measurements at Ulan Baatar, Mongolia, *Geophys. Res. Lett.,* **27,** 1527–1531

Calais, E., Vergnolle, M., Sankov, V., Lukhnev, A., Miroshnitchenko, A., Amarjargal, S. & Deverchere, J., 2003. GPS measurements of crustal deformation in the Baikal-Mongolia area (1994–2002): implications for current kinematics of Asia, *J. geophys. Res.,* **108,** doi:10.1029/2002JB002373.

Chamot-Rooke, N. & Le Pichon, X., 1999. GPS determined eastward Sundaland motion with respect to Eurasia confirmed by earthquakes slip vectors at Sunda and Philippine trenches, *Earth planet. Sci. Lett.,* **173,** 439–455.

Chen, W.P. & Nabelek, J., 1988. Seismogenic strike-slip faulting and the development of the North China basin, *Tectonics,* **7,** 975–989.

Crétaux, J.-F., Soudarin, L., Cazenave, A. & Bouillé, F., 1998. Present-day tectonic plate motions and crustal deformations from the DORIS space system, *J. geophys. Res.,* **103,** 30 167–30 181.

Dziewonski, A.M., Ekström G. & Maternovskaya, N.N., 2003. Centroid-moment tensor solutions for October–December 2000, *Phys. Earth planet. Int.,* **136,** 145–163.

England, P.C. & Houseman, G.A., 1986. Finite strain calculations of continental deformation, 2, comparison with the India–Asia collision zone, *J. geophys. Res.,* **91,** 3664–3676.

England, P.C. & Molnar, P., 1997. The field of crustal velocity in Asia calculated from Quaternary rates of slip on faults, *Geophys. J. Int.,* **130,** 555–582.

Flesch, L.M., Holt, W.E. & Haines, A.J., 2001. Dynamics of the India–Asia collision zone, *J. geophys. Res.,* **106,** 16 435–16 460.

Fournier, M., Jolivet, L., Huchon, P., Rozhdestvensky, V.S., Sergeyev, K.F. & Oscorbin, L., 1994. Neogene strike-slip faulting in Sakhalin, and the Japan Sea opening, *J. geophys. Res.,* **99,** 2701–2725.

Fournier, M., Jolivet, L., Davy, P. & Thomas, J.-C., 2004. Back arc extension and collision : an experimental approach of the tectonics of Asia, *Geophys. J. Int.,* **157,** 871–889.

Heki, K., 1996. Horizontal and vertical crustal movements from three-dimensional very long baseline interferometry kinematic reference frame: implication for the reversal timescale revision, *J. geophys. Res.,* **101,** 3187–3198.

Heki, K. & Miyazaki, S., 2001. Plate convergence and long-term crustal deformation in Central Japan, *Geophys. Res. Lett.,* **28,** 2313–2316.

Heki, K. *et al.,* 1999. The Amurian Plate motion and current plate kinematics in eastern Asia, *J. geophys. Res.,* **104,** 29 147–29 155.

Hellinger, S.J., Shedloock, K.M., Sclater, J.G. & Hong, Y., 1985. The Cenozoic evolution of the north China basin, *Tectonics,* **4,** 343–358.

Holt, W.E., Chamot-Rooke, N., Le Pichon, X., Haines, A.J., Shen-Tu, B. & Ren, J., 2000. Velocity field in Asia inferred from Quaternary fault slip rates and Global Positioning System observations, *J. geophys. Res.,* **105,** 19 185–19 209.

Holt, W.E., Li, M. & Haines, A.J., 1995. Earthquake strain rates and instantaneous relative motions within central and eastern Asia, *Geophys. J. Int.,* **122,** 569–593.

Houseman, G.A. & England, P.C., 1993. Crustal thickening versus lateral expulsion in the India–Asian continental collision, *J. geophys. Res.,* **98,** 12 233–12 249.

Jestin, F., Huchon, P., Gaulier, J.M., 1994. The Somalia plate and the East African rift system: present-day kinematics, *Geophys. J. Int.,* **116,** 637–654.

Jolivet, L. & Tamaki, K., 1992. Neogene kinematics in the Japan Sea region and the volcanic activity of the Northeast Japan arc, *Proc. ODP Sci. Results,* **127/128**(2), 1311–1331.

Jolivet, L., Fournier, M., Huchon, P., Rozhdestvenskiy, S., Sergeyev, K. & Oscorbin, L., 1992. Cenozoic intracontinental dextral motion in the Okhotsk-Japan Sea region, *Tectonics,* **12,** 968–977.

Kong, X. & Bird, P., 1996. Neotectonics of Asia: thin-shell finite element models with faults, in *The Tectonic Evolution of Asia,* pp.18–34, eds Yin, A. & Harrison, T.M., Cambridge University Press, Cambridge.

Kreemer, C., Holt, W. & Haines, A.J., 2003. An integrated global model of present-day plate motions and plate boundary deformation, *Geophys. J. Int.,* **154,** 8–34.

Larson, K.M., Bürgmann, R., Bilham, R. & Freymueller, J.T., 1999. Kinematics of the India–Eurasia collision zone from GPS measurements, *J. geophys. Res.,* **104,** 1077–1093.

Logatchev, N.A. & Zorin, Y.A., 1987. Evidences and causes of the two-stages development of the Baikal rift, *Tectonophysics,* **143,** 225–234.

Lysak, S.V., 1992. Heat flow variations in continental rifts, *Tectonophysics,* **208,** 309–323.

Mazzotti, S., Henry, P. & Le Pichon, X., 2001. Transient and permanent deformation of central Japan estimated by GPS. 2. Strain partitioning and arc–arc collision, *Earth planet. Sci. Lett.,* **184,** 455–469.

Molnar, P. & Deng, Q., 1984. Faulting associated with large earthquakes and the average rate of deformation in central and eastern Asia, *J. geophys. Res.,* **89,** 6203–6227.

Molnar, P. & Gipson, J.M., 1996. A bound on the rheology of continental lithosphere using very long baseline interferometry: the velocity of south China with respect to Eurasia, *J. geophys. Res.,* **101,** 545–554.

Nakamura, K., 1983. Possible nascent trench along the eastern Japan Sea as the convergent boundary between Eurasia and North American plates, *Bull. Earthquake Res. Inst. Univ. Tokyo,* **58,** 711–722 [in Japanese].

Parfenov, L.M., Koz'min, B.M., Imayev, V.S. & Savostin, L.A., 1987. The tectonic character of the Olekma-Stanovoy seismic zone, *Geotectonics,* **21,** 560–572.

Peltzer, G. & Saucier, F., 1996. Present-day kinematics of Asia derived from geologic fault rates, *J. geophys. Res.,* **101,** 27 943–27 956.

Petit, C., Déverchère, J., Houdry, F., Sankov, V.A., Melnikova, V.I. & Delvaux, D., 1996. Present-day stress field changes along the Baikal rift and tectonic implications, *Tectonics,* **15,** 1171–1191.

Pollack, H.N., Hurter, S.J. & Johnson, J.R., 1993. Heat flow from the Earth's interior: analysis of the global data set, *Rev. Geophys.,* **31,** 267–280.

Polyansky, O.P., 2002. Dynamic causes for the opening of the Baikal rift zone: a numerical modelling approach, *Tectonophysics,* **351,** 91–117.

Reinecker, J., Heidbach, O. & Mueller, B., 2003. *World Stress Map* (available on-line at www.world-stress-map.org).

Ritz, J.F., Brown, E.T., Boulés, D.L., Philip, H., Schlupp, A., Raisbeck, G.M., Yiou, F. & Enkhtuvshin, B., 1995. Slip rates along active faults estimated with cosmic-ray-exposure dates: application to the Bogd fault, Gobi-Altaï, Mongolia, *Geology,* **23,** 1019–1022.

Sagiya, T., Miyazaki, S. & Tada, T., 2000. Continuous GPS array and present-day crustal deformation in Japan, *Pure appl. Geophys.,* **157,** 2303–2322.

Sella, G., Dixon, T.H. & Mao, A., 2002. REVEL: a model for recent plate velocities from space geodesy, *J. geophys. Res.,* **107,** doi:10.1029/2000JB000033.

Seno, T., Sakurai T. & Stein, S., 1996. Can the Okhotsk plate be discriminated from the North American plate?, *J. geophys. Res.,* **101,** 11 305–11 315.

Shen, Z.-K., Zhao, C., Yin, A., Li, Y., Jackson, D.D., Fang, P. & Dong, D., 2000. Contemporary crustal deformation in east Asia constrained by Global Positioning System measurements, *J. geophys. Res.,* **105,** 5721–5734.

Takahashi, H. *et al.,* 1999. Velocity field around the Sea of Okhotsk and Sea of Japan regions determined by a new continuous GPS network data, *Geophys. Res. Lett.,* **26,** 2533–2536.

Tamaki, K. & Honza, E., 1984. Incipient subduction and obduction along the eastern margin of the Japan Sea, *Tectonophysics,* **119,** 381–406.

Tamaki, K., Suyehiro, K., Allan, J., Ingle, J.C. & Pisciotto, K., 1992. Tectonic synthesis and implications of Japan Sea ODP drilling, *Proc. ODP Sci. Results,* **127**/**128**(2), 1333–1350.

Tapponnier, P., Peltzer, G., Le Dain, A.Y. & Armijo, R., 1982. Propagating extrusion tectonics in Asia: new insights from simple experiments with plasticine, *Geology,* **10,** 611–616.

Vergnolle, M. & Calais, E., 2003. Deformation model of Central Asia constrained by a GPS-derived velocity field in Mongolia and China, *EGS–EUG–AGU Joint Assembly, Nice, April 6–11*. Abstract EAE03-A-02343, 2003, p. 384.

Wang, Q. *et al.,* 2001. Present-day crustal deformation in China constrained by Global Positioning System measurements, *Science,* **294,** 574–577.

Weaver, R., Roberts, A.P., Flecker, R., Macdonald, D.I., & Fot'yanova, L.M., 2003. Geodynamic implications of paleomagnetic data from Tertiary sediments in Sakhalin, Russia (NW Pacific), *J. geophys. Res.,* **108,** 2066 doi:10.1029/2001JB001226.

Wei, D.-P. & Seno, T., 1998. Determination of the Amurian plate motion, in *Mantle Dynamics and Plate Interactions in East Asia,* AGU Geodynamics Series 27, p. 419, eds Flower, M.F.J., Chung, S.-L., Lo, C.-H. & Lee, T.-Y., American Geophysical Union, Washington, DC.

Zhang, Y.Q., Mercier, J.-L. & Vergély, P., 1998. Extension in the graben systems around the Ordos (China), and its contribution to the extrusion tectonics of south China with respect to Gobi-Mongolia, *Tectonophysics,* **285,** 41–75.

Zoback, M.L., 1992. First- and second-order patterns of stress in the lithosphere: the World Stress Map Project, *J. geophys. Res.,* **97,** 11 703–11 728.

Zonenshain, L.P. & Savostin, L.A., 1981. Geodynamics of Baikal rift zone and plate tectonics of Asia, *Tectonophysics,* **76,** 1–45.